Monthly Notices
of the
ROYAL ASTRONOMICAL SOCIETY

Mon. Not. R. Astron. Soc. **404,** 1396–1414 (2010) doi:10.1111/j.1365-2966.2010.16353.x

Mopra line survey mapping of NGC 6334 I and I(N) at 3 mm

A. J. Walsh,[1,2⋆] S. Thorwirth,[3,4] H. Beuther[5] and M. G. Burton[1]

[1] *School of Physics, University of New South Wales, Sydney, 2052 NSW, Australia*
[2] *Centre for Astronomy, School of Engineering and Physical Sciences, James Cook University, Townsville, QLD 4811, Australia*
[3] *I. Physikalisches Institut, Universität zu Köln, Zülpicher Str. 77, 50937 Köln, Germany*
[4] *Max-Planck-Institut für Radioastronomie, Auf dem Hügel 69, 53121 Bonn, Germany*
[5] *Max-Planck-Institut für Astronomie, Königstuhl 17, 69117 Heidelberg, Germany*

Accepted 2010 January 13. Received 2009 November 15; in original form 2009 July 23

ABSTRACT

A 5 × 5 arcmin^2 region encompassing NGC 6334 I and I(N) has been mapped at a wavelength of 3 mm (from 83.5 to 115.5 GHz) with the Mopra telescope at an angular resolution between 33 and 36 arcsec. This investigation has made use of the recently installed 3 mm Monolithic Microwave Integrated Circuit (MMIC) receiver and the Mopra Spectrometer with broad-band capabilities permitting total coverage of the entire frequency range with just five different observations. In total, the spatial distributions of 19 different molecules, ions and radicals, along with additional selected isotopologues, have been studied. Whilst most species trace the sites of star formation, CH_3CN appears to be most closely associated with NGC 6334 I and I(N). Both CN and C_2H appear to be widespread, tracing gas that is not associated with active star formation. Both N_2H^+ and HC_3N closely resemble dust continuum emission, showing that they are reliable tracers of dense material as well as the youngest stages of high-mass star formation. Hot ($E_u/k > 100$ K) thermal CH_3OH emission is preferentially found towards NGC 6334 I, contrasting with I(N), where only cold ($E_u/k < 22$ K) thermal CH_3OH emission is found.

Key words: circumstellar matter – infrared: stars.

1 INTRODUCTION

NGC 6334 is a giant molecular cloud located at a distance of 1.7 kpc (Neckel 1978) in the southern Galactic plane. Lying along a gas filament of 11 pc in length, NGC 6334 exhibits several luminous sites of massive star formation – as seen in the far-infrared (McBreen et al. 1979; five sources denoted using roman numerals I to V) and radio continuum (Rodriguez, Canto & Moran 1982; six sources denoted with letters from A to F) with source I dominating the millimetre to the far-infrared (Sandell 2000). In close proximity to NGC 6334 I, about 2 arcmin to the north, another bright source is found in the millimetre and submillimetre continuum, denoted NGC 6334 I(N) (Cheung et al. 1978; Gezari 1982; Sandell 2000). While this source is believed to be a comparably young object – as concluded from the lack of H II regions and mid-IR emission – there is compelling evidence, however, that star formation is going on there (e.g. Megeath & Tieftrunk 1999). It is this twin core system, NGC 6334 I and I(N), that offers the rare opportunity to study the evolution of high-mass stars from the same parental cloud and in a relatively small spatial region.

Single-dish molecular line observations show both cores to be chemically rich (Thorwirth et al. 2003) with source I being comparable in line density to prototypical hot cores such as Orion-KL and SgrB2(N) (Bachiller & Cernicharo 1990; McCutcheon et al. 2000; Thorwirth et al. 2003; Schilke et al. 2006). High spatial resolution observations towards both cores have been conducted: Australia Telescope Compact Array (ATCA) investigations of NH_3 emission up to the (6, 6) inversion transition reveals the presence of warm gas in both cores (Beuther et al. 2005, 2007) and Submillimeter Array continuum observations at 1.3 mm (Hunter et al. 2006) resolve each core into a sample of sub-cores of several tens of solar masses each, four for source I and seven for I(N), demonstrating the formation of star clusters.

Several line mapping studies using standard molecular tracers were carried out in the past to obtain information about the large-scale spatial distribution of molecular gas (Kraemer & Jackson 1999; McCutcheon et al. 2000), additionally leading to the detection of several molecular outflows associated with both cores (Bachiller & Cernicharo 1990; Megeath & Tieftrunk 1999; Leurini et al. 2006).

In the present investigation, we have used the Mopra telescope for spectral line mapping of a 5 × 5 arcmin^2 region around NGC 6334 I and I(N) throughout the entire 3 mm range.

⋆E-mail: Andrew.Walsh@jcu.edu.au

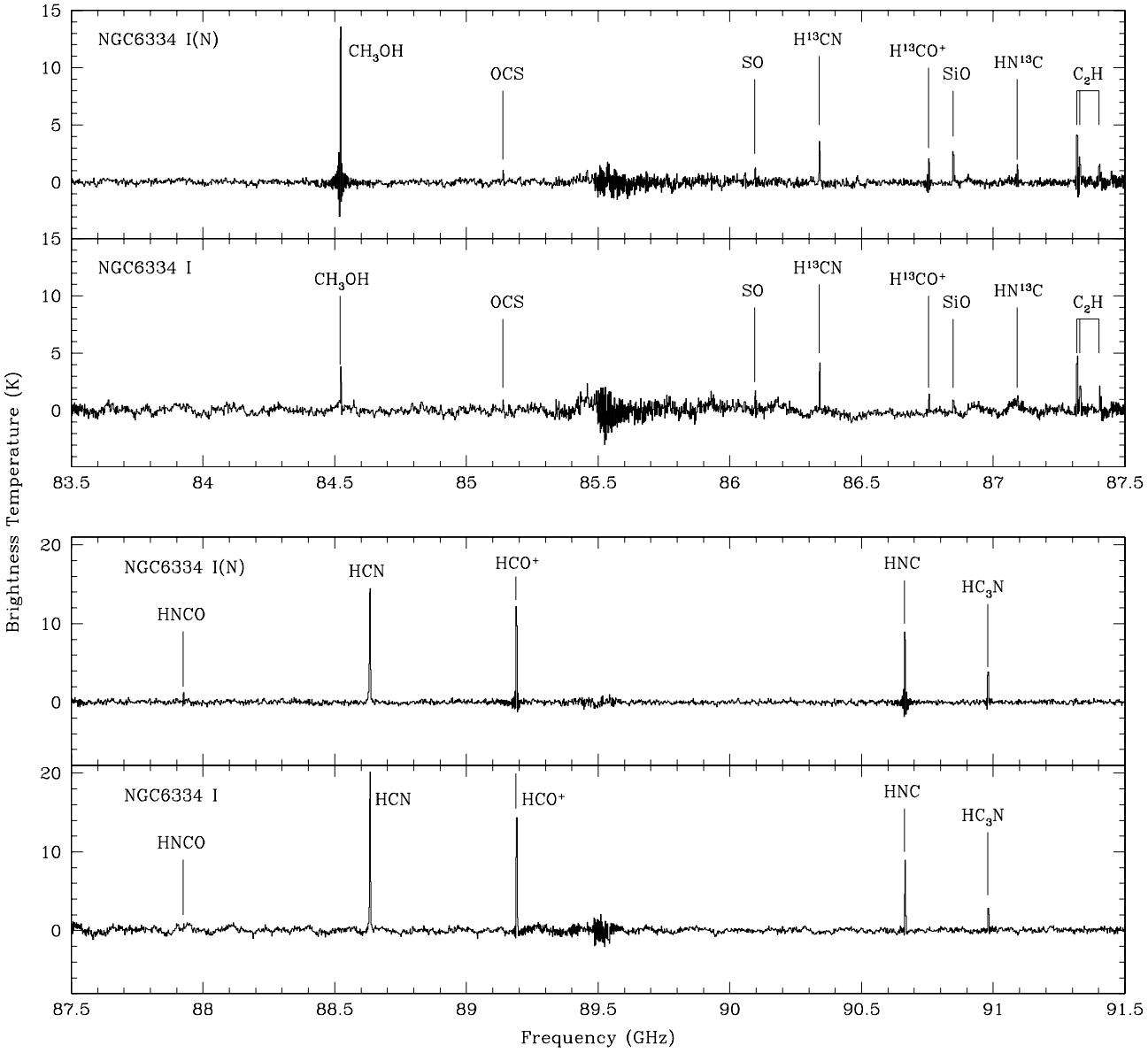

Figure 1. Spectra of NGC 6334 I (lower) and NGC 6334 I(N) (upper) shown between 83.5 and 91.5 GHz. The frequencies of identified lines in each spectrum are indicated with a solid vertical line. Each spectrum was produced by integrating over a square box with each side approximately equal to the beam width (36 arcsec). Strong lines in the spectrum occasionally produce a ringing artefact close to the line frequency, e.g. CH_3OH in I(N). This is a result of the Gibbs phenomenon and is most pronounced with narrow lines, such as masers. The frequency range is between 91.5 and 99.5 GHz. The frequency range is between 99.5 and 107.5 GHz. The large blank areas shown on the upper plot are because the data in these frequency ranges were unfortunately unusable. Note that one line appears at approximately 100.322 GHz. This is a reflection of HNC at 90.664 GHz, and not a real line. The frequency range is between 107.5 and 115.5 GHz. The frequencies of identified lines in each spectrum are indicated with a solid vertical line below the spectrum.

2 OBSERVATIONS

Observations were carried out in 2006 June 25, using the 22 m Mopra telescope near Coonabarabran, New South Wales, Australia.[1] We used the recently commissioned 3 mm MMIC receiver in combination with the new Mopra Spectrometer (MOPS) in a broad-band mode[2] resulting in an instantaneous bandwidth of 8 GHz split over four overlapping intermediate frequencies (IFs) of 2.2 GHz each. At the time of the observations MOPS provided 1024 channels per IF, giving a total of 8192 channels. The spectral resolution of the observations was 2 MHz corresponding to a velocity resolution of about 6 km s^{-1} per channel. For NGC 6334,

[1] For detailed information on the facility, visit the Mopra website page at http://www.narrabri.atnf.csiro.au/mopra/

[2] Detailed information on the available receivers and backends can be found online in the 'Technical Summary of the Mopra Radiotelescope' available at http://www.narrabri.atnf.csiro.au/mopra/mopragu.pdf

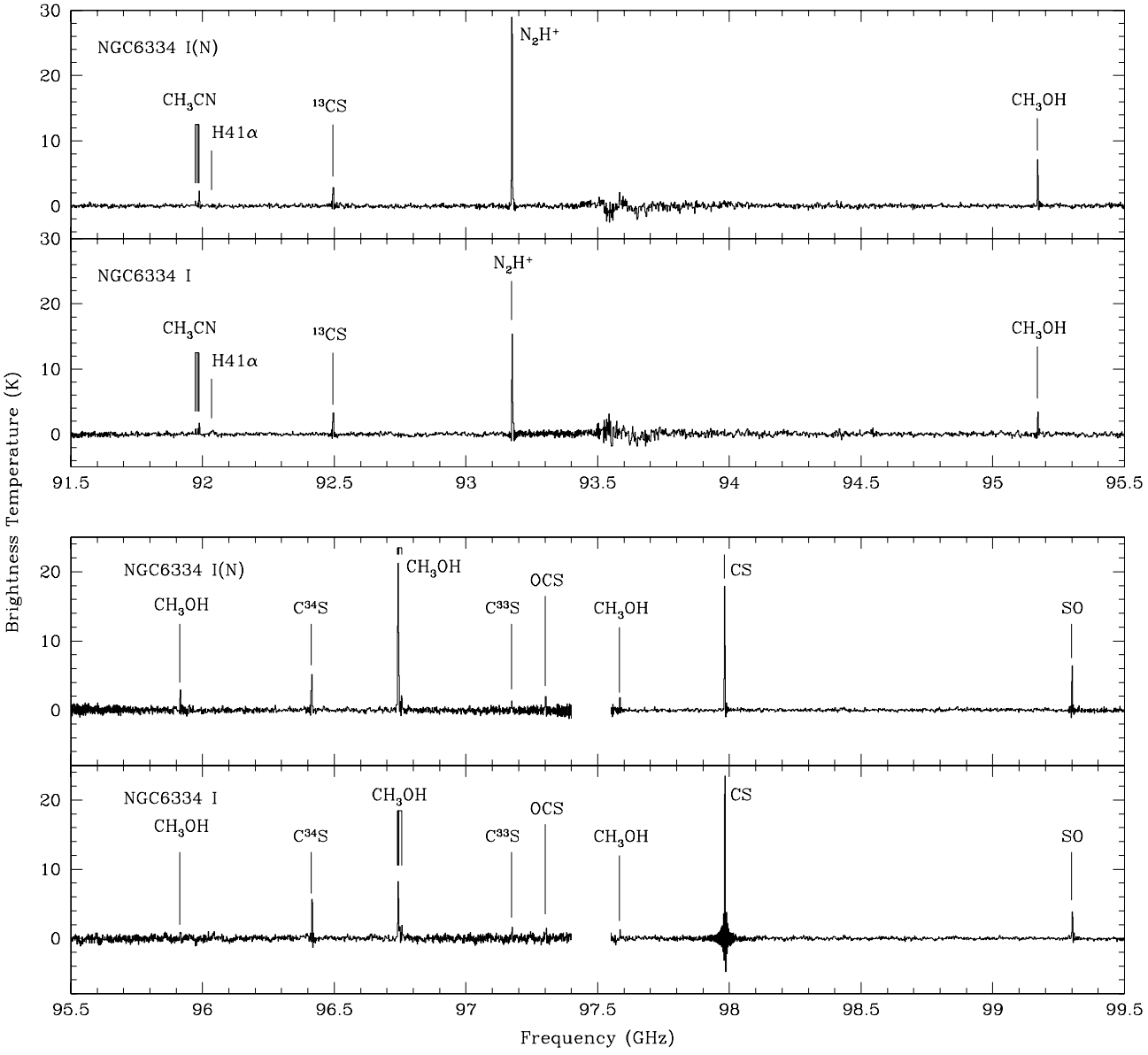

Figure 1 – *continued*

this velocity resolution is about the same or slightly larger than the expected linewidths, which means that while we do not expect to spectrally resolve many lines, we will not suffer a significant loss in signal due to spectral smearing. Thus, this work will necessarily concentrate on morphologies and integrated intensities of emission, rather than any analysis of kinematic structure.

The pointing centre for the maps was chosen to be RA(J2000) = $17^{h}20^{m}54\overset{s}{.}24$, Dec. (J2000) = $-35^{\circ}46'11\overset{''}{.}5$, which is approximately half-way between NGC 6334 I and I(N). We used the on-the-fly mapping routine to map an area of 5×5 arcmin^2 around this position. Due to incomplete sampling of the edges of the map, a slightly smaller area is considered in this work. A scanning rate of 3.5 arcsec s^{-1} was used. Data were averaged every 2 s which gives an optimum data collection rate with minimal smearing of the output. A spacing of 10 arcsec was used between each scanning row. Assuming a beam of between 33 and 36 arcsec, depending on the frequency (Ladd et al. 2005), this observing mode resulted in a fully sampled map. A single map was obtained in about 90 min, including about 15 per cent of this time for T_{SYS} calibration, reference observations and pointing on a nearby SiO maser (AH Sco). Poor weather (clouds) affected some of the data, which usually appears as faint horizontal stripes in the data (see the following sections for details).

3 RESULTS

Fig. 1 shows spectra at I and I(N) across the 3 mm band. Each spectrum was made by integrating the emission over a box approximately equal to the size of the beam. The spectrum for NGC 6334 I was centred on the methanol maser site that overlaps with the UC H II region ($17^{h}20^{m}53\overset{s}{.}35$, $-35^{\circ}47'1\overset{''}{.}6$) and the spectrum for NGC 6334 I(N) was centred on the methanol maser site ($17^{h}20^{m}54\overset{s}{.}58$, $-35^{\circ}45'8\overset{''}{.}6$). Across the band, we detect a total of 52 transitions from 19 species. Details of each detection are given in Table 1.

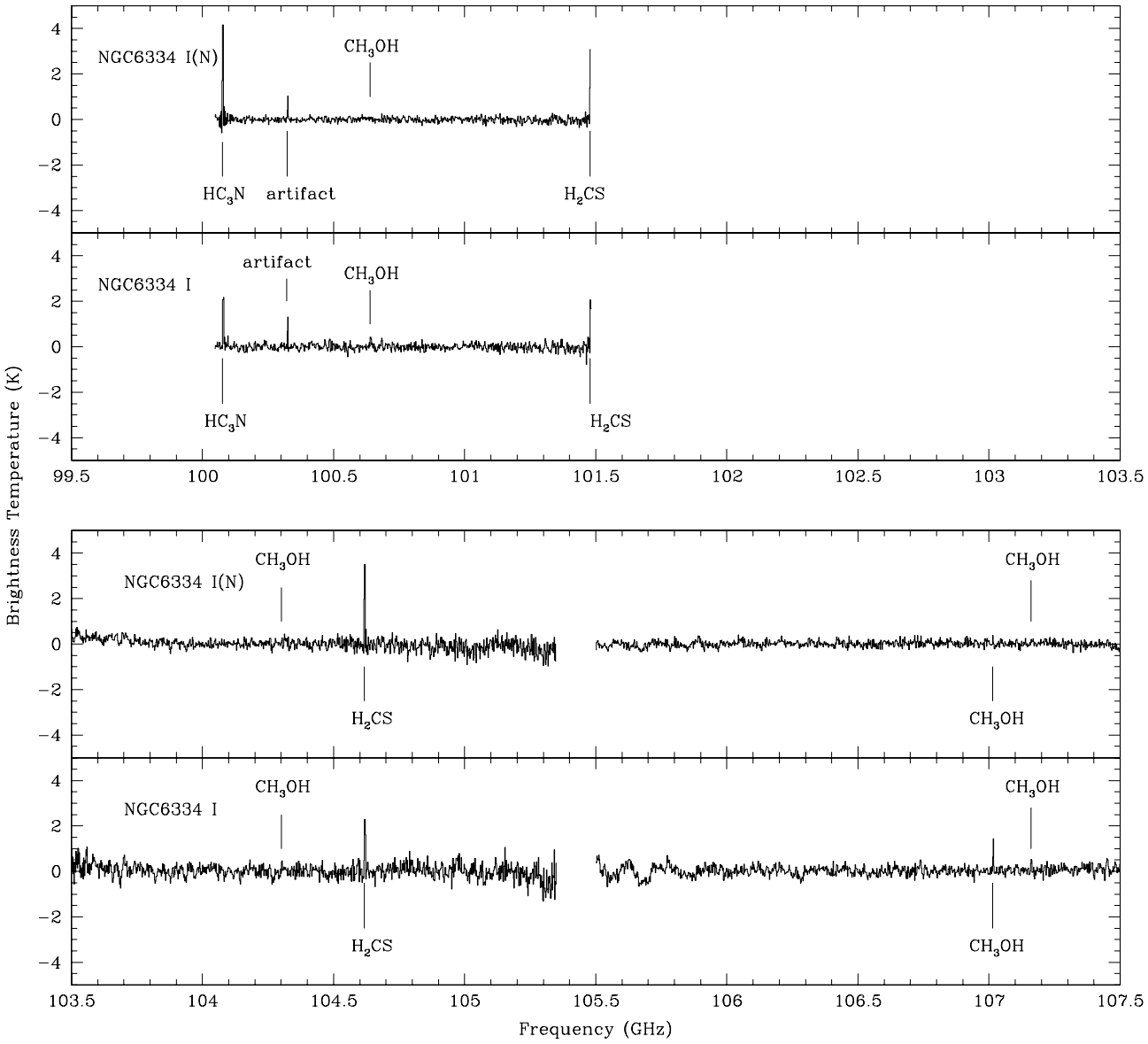

Figure 1 – *continued*

Fig. 2 shows dust continuum emission in the region taken using Submillimetre Common-User Bolometer Array (SCUBA) on the James Clerk Maxwell Telescope (JCMT) (Sandell, private communication). These images were taken on 1998 June 26 and July 1, with measured half-power beam widths of 14.6 arcsec at 850 μm and 8 arcsec at 450 μm, respectively. In this figure, the plus symbols represent the positions of methanol maser emission (Walsh et al. 1998). In the north, the methanol maser site marks the position of NGC 6334 I(N). In the south, two maser sites are seen, spaced about 7 arcsec apart. Coincident with one of these maser sites and marked by the diamond is the UC H II region NGC 6334 I. The other, nearby maser site marks the position of a hot core (e.g. Beuther et al. 2005). The circle marks the position and approximate extent of the H II region NGC 6334 E. Strong sources of sub-mm continuum emission appear associated with both NGC 6334 I and NGC 6334 I(N). At the position of NGC 6334 I, the dust continuum appears to peak at the UC H II region position, rather than the hot core located to the north-west. The continuum emission also appears to be essentially unresolved here. Higher resolution observations by Hunter et al. (2006) show that the continuum emission does fragment into multiple sources.

The continuum emission associated with NGC 6334 I appears to be extended over almost an arcminute, corresponding to a projected length of nearly 0.5 pc. The continuum emission also appears to peak about 6 arcsec to the south-east of the maser site associated with NGC 6334 I(N). The grey-scale continuum images also show the low-level dust emission, which exhibits a prominent filamentary structure running from the south-western corner to the centre-top of the field of view. Other, weaker filamentary structures appear as a bridge between NGC 6334 I and I(N), as well as possibly connecting NGC 6334 I and NGC 6334 E, although very little continuum emission is coincident with the H II region NGC 6334 E. The very weak filamentary structure appears to extend from NGC 6334 I(N) to the north-eastern corner of the field of view. Finally, there is some

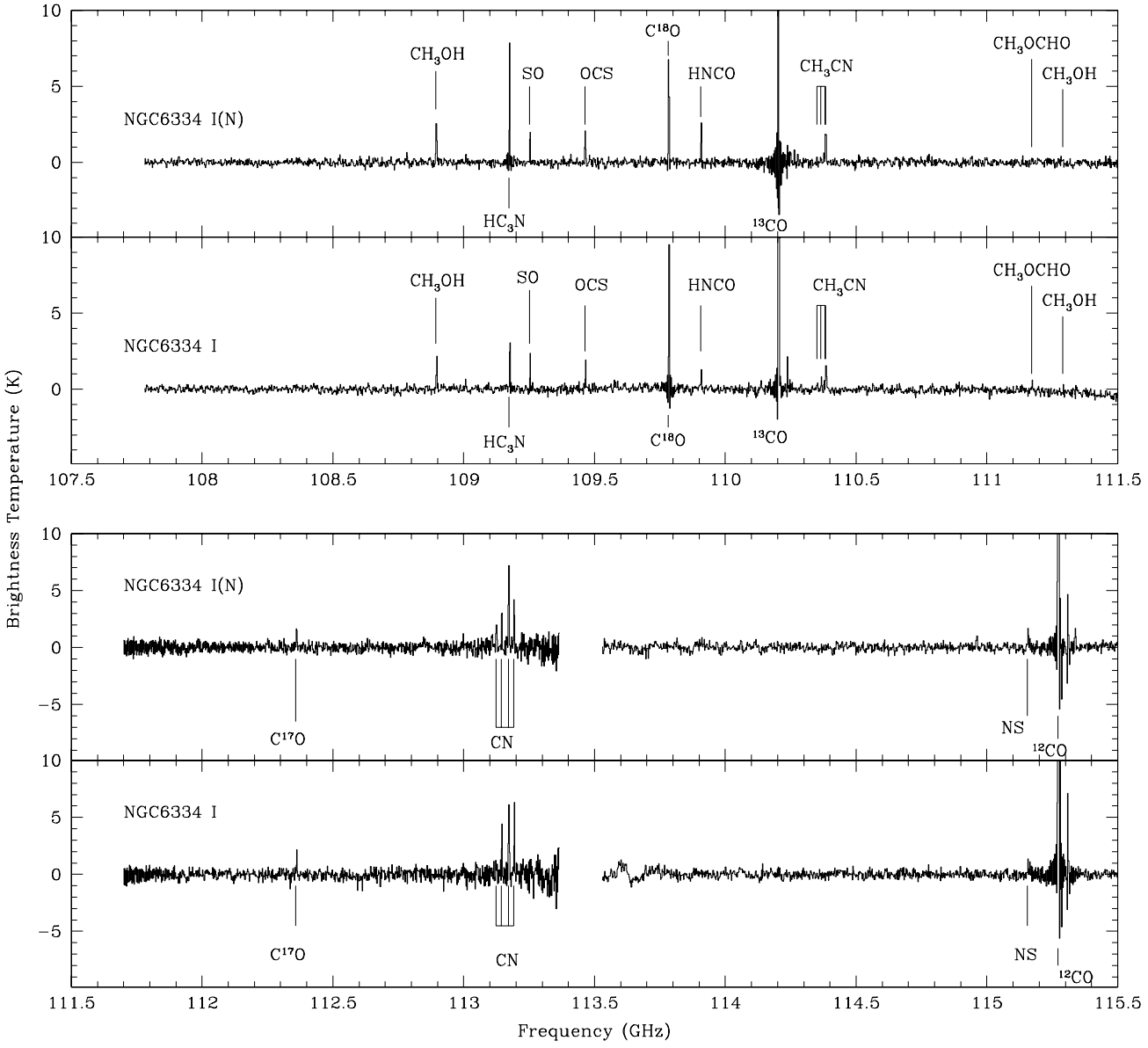

Figure 1 – *continued*

emission seen directly to the north of NGC 6334 I(N), which may be an extension of the filament seen to bridge the gap between NGC 6334 I and I(N).

4 DISCUSSION

4.1 Morphological analysis

Since the spectral resolution was relatively coarse, we refrain from an analysis of spectrally resolved data cubes and only show and interpret integrated images of the different molecular species and isotopologues, as shown in Fig. 3. Furthermore, the angular resolution of the Mopra telescope in the 3 mm band is ∼36 arcsec (at 90 GHz) corresponding to a linear resolution of ∼65 000 au or ∼0.3 pc. This spatial resolution is not sufficient to analyse spatial differences within one or the other massive star-forming region. However, it allows us to investigate the molecular global properties, similarities and differences between the different massive star-forming regions present in our field of view. In the following, we will qualitatively describe the global spatial characteristics of the different molecular species and its isotopologues.

H41α. This is the only covered hydrogen recombination line that we could image and is found as expected towards the UC H II region associated with NGC 6334 I.

C_2H. C_2H shows a peculiar spatial morphology since its main emission peak is associated with NGC 6334 I(N) and appears as a weak hole at the position of NGC 6334 E. Furthermore, extended emission closely follows the dust continuum ridge shown in Fig. 2. This molecule shows no clear peak towards the southern source NGC 6334I. The dearth of emission coincident with both NGC 6334 E and I suggests that this molecule is destroyed close to H II region environments.

Unsaturated hydrocarbons such as C_2H are known to be strong at early evolutionary stages (e.g. Millar & Nejad 1985; Turner, Terzieva & Herbst 1999). During the warm-up of the cores, it reacts quickly with oxygen to form CO through ion–molecule chemistry

Table 1. Molecular lines mapped towards the NGC 6334 I/I(N) region in the present study. Transition frequencies (MHz) were taken from the Cologne Database for Molecular Spectroscopy (Müller et al. 2001, 2005) in most cases and the Jet Propulsion Laboratory catalogue (Pickett et al. 1998). Also given are the integrated intensities for each transition, as measured at NGC 6334 I and I(N) by integrating the emission over one beam, as was done for the spectra presented in Fig. 1. 3σ upper limits are given for those transitions not detected.

Molecule	Transition	Frequency (MHz)	Methanol maser class	Integrated intensity (K km s^{-1})	
				NGC 6334 I	NGC 6334 I(N)
H	41α	92 034.442		26	$<10^a$
C_2H	$N = 1$–0, $J = 3/2$–$1/2$, $F = 2$–1	87 316.898		66	60
C_2H	$N = 1$–0, $J = 3/2$–$1/2$, $F = 1$–0	87 328.585		38	32
C_2H	$N = 1$–0, $J = 1/2$–$1/2$, $F = 1$–1	87 401.989		35^b	23^b
CN	$N = 1$–0, $J = 1/2$–$1/2$, $F = 1/2$–$1/2$	113 123.370		8.9	19
CN	$N = 1$–0, $J = 1/2$–$1/2$, $F = 1/2$–$3/2$	113 144.157		38	34
CN	$N = 1$–0, $J = 1/2$–$1/2$, $F = 3/2$–$1/2$	113 170.492		61	64
CN	$N = 1$–0, $J = 1/2$–$1/2$, $F = 3/2$–$3/2$	113 191.279		56	46
$H^{13}CN$	$J = 1$–0	86 339.922		61	57
HCN	$J = 1$–0	88 631.602		350	300
$HN^{13}C$	$J = 1$–0	87 090.850		19	20
HNC	$J = 1$–0	90 663.568		100	110
$C^{18}O$	$J = 1$–0	109 782.173		69	69
^{13}CO	$J = 1$–0	110 201.354		360	350
$C^{17}O$	$J = 1$–0	112 359.284		19	21
^{12}CO	$J = 1$–0	115 271.202		930	680
N_2H^+	$J = 1$–0	93 173.392		210	440
$H^{13}CO^+$	$J = 1$–0	86 754.288		16	24
HCO^+	$J = 1$–0	89 188.525		170	150
CH_3OH-E	$J_{K_a,K_c} = 5_{-1,5}$–$4_{0,4}$	84 521.169	I	80	180
CH_3OH-A^+	$J_{K_a,K_c} = 8_{0,8}$–$7_{1,7}$	95 169.463	I	41	88
CH_3OH-A^+	$J_{K_a,K_c} = 2_{1,2}$–$1_{1,1}$	95 914.309		16	32
CH_3OH-A^+	$J_{K_a,K_c} = 2_{0,2}$–$1_{0,1}$	96 741.375		150	370
CH_3OH-A^-	$J_{K_a,K_c} = 2_{1,1}$–$1_{1,0}$	97 582.804		9.5	24
CH_3OH-E	$J_{K_a,K_c} = 13_{2,11}$–$12_{3,9}$	100 638.900		4.9	$<0.9^a$
CH_3OH-E	$J_{K_a,K_c} = 11_{-1,11}$–$10_{-2,9}$	104 300.414	I	5.5	$<1.8^a$
CH_3OH-A^+	$J_{K_a,K_c} = 3_{1,3}$–$4_{0,4}$	107 013.803	II	15	2.7
CH_3OH-E	$J_{K_a,K_c} = 15_{-2,14}$–$15_{1,14}$	107 159.820		8.2	$<1.8^a$
CH_3OH-E	$J_{K_a,K_c} = 0_{0,0}$–$1_{-1,1}$	108 893.963	II	18	28
CH_3OH-A^+	$J_{K_a,K_c} = 7_{2,5}$–$8_{1,8}$	111 289.550		1.9	$<1.2^a$
CH_3CN	$J_K = 5_0$–4_0	91 987.091		41^c	35^c
CH_3CN	$J_K = 5_1$–4_1	91 985.318			
CH_3CN	$J_K = 5_2$–4_2	91 979.998			
CH_3CN	$J_K = 5_3$–4_3	91 971.134			
CH_3CN	$J_K = 6_0$–5_0	110 383.504		30^d	32^d
CH_3CN	$J_K = 6_1$–5_1	110 381.376			
CH_3CN	$J_K = 6_2$–5_2	110 374.993			
CH_3CN	$J_K = 6_3$–5_3	110 364.358			
HNCO	$J_{K_a,K_c} = 4_{0,4}$–$3_{0,3}$	87 925.237		$<1.8^a$	25
HNCO	$J_{K_a,K_c} = 5_{0,5}$–$4_{0,4}$	109 905.749		12	23
^{13}CS	$J = 2$–1	92 494.308		36	32
$C^{34}S$	$J = 2$–1	96 412.950		73	61
$C^{33}S$	$J = 2$–1	97 172.064		21	14
CS	$J = 2$–1	97 980.953		290	210
SiO	$J = 2$–1	86 846.960		13	41
NS	$^2\Pi_{1/2}$ $N = 2$–1, $J = 5/2$–$3/2$ $F = 7/2$–$5/2$, c-state	115 153.835		8.5	17
H_2CS	$J_{K_a,K_c} = 3_{1,3}$–$2_{1,2}$	101 477.810		>24	>20
H_2CS	$J_{K_a,K_c} = 3_{1,2}$–$2_{1,1}$	104 617.040		27	34
SO	$N_J = 2_2$–1_1	86 093.950		22	19
SO	$N_J = 2_3$–1_2	99 299.870		53	69
SO	$N_J = 3_2$–2_1	109 252.220		18	21
HC_3N	$J = 10$–9	90 979.023		38	48
HC_3N	$J = 11$–10	100 076.392		27	38
HC_3N	$J = 12$–11	109 173.634		33	59

Table 1 – *continued*

Molecule	Transition	Frequency (MHz)	Methanol maser class	Integrated intensity (K km s^{-1}) NGC 6334 I	NGC 6334 I(N)
OCS	$J = 7$–6	85 139.103		12	17
OCS	$J = 8$–7	97 301.209		19	19
OCS	$J = 9$–8	109 463.063		19	25
CH_3OCHO^e	$J_{K_a,K_c} = 10_{0,10}$–$9_{0,9}$	111 171.636		4.5	$<0.9^a$

[a] 3σ upper limit.
[b] Blend with C_2H $N = 1$–0, $J = 1/2$–$1/2$, $F = 0$–1 at 87 407.165 MHz.
[c] Integrated emission for all $J = 5$–4 transitions.
[d] Integrated emission for all $J = 6$–5 transitions.
[e] Blend of A and E types.

(e.g. Herbst & Leung 1986; Turner et al. 1999). These models are consistent with our finding of the C_2H peak close to NGC 6334 I(N) and much less emission towards the hot core NGC 6334 I or the H II region NGC 6334 E. Furthermore, Beuther et al. (2008) confirm that during ongoing evolution C_2H abundances decrease towards star formation sites. Thus, C_2H is a good tracer of gas that is not directly associated with active star formation.

CN. The radical CN appears to be smoothly distributed over a region covering NGC 6334 I, E and I(N). One transition is slightly stronger at NGC 6334 I and the other is slightly stronger at NGC 6334 I(N). However, these are weak peaks over the extended emission and so it is not possible to tell if the difference in relative intensities is real or due to noise variations. CN, like C_2H, appears to be a good tracer of gas not directly associated with active star formation.

^{12}CO, ^{13}CO, C^{18}O and C^{17}O. Carbon monoxide and its isotopologues are easily detected in our field of view. However, the spatial distribution is surprising because it does not trace clearly any of the two main massive star-forming regions, NGC 6334 I or I(N). The main emission peak is located approximately 50 arcsec north-west of NGC 6334 I, closer to the UC H II region NGC 6334 E (but not coincident). We note that this peak does not appear pronounced in any other spectral line imaged in this work nor does it feature prominently in the dust continuum map. Since only CO (1–0) transitions are prominent at this position ($17^h20^m48^s.45$, $-35^\circ46'30''$) and these transitions have a low effective critical density ($\sim 10^2$ cm^{-3}), we believe that this line of sight contains a high column density of low density gas without any significant high density centre that might contain star formation. While ^{12}CO, ^{13}CO and C^{18}O show weaker secondary peaks towards NGC 6334 I and I(N), these are barely detectable in the rarest isotopologue C^{17}O. Based on the mm continuum maps (e.g. Sandell 2000, see also Fig. 2) it is obvious that the highest gas column densities are towards NGC 6334 I and I(N); therefore, non-detection of these peaks in rare CO isotopologues cannot be explained by column density effects. The temperatures towards NGC 6334 I and I(N) exceed 100 K (Beuther et al. 2005) whereas the excitation temperatures of the upper energy levels of the $J = 1$–0 carbon monoxide transitions are only of the order of 5 K. With a typical Boltzmann distribution, one would expect, for example, the $J = 6$–5 transitions to peak closer to the warm regions NGC 6334 I and I(N).

An additional interesting feature in the CO maps is the more extended north–south ridge. It would be useful to have larger maps to investigate to what extent this ridge is continuing, but a comparison with the mm continuum map indicates that this CO ridge has no direct counterpart in the dense gas and dust component.

N_2H^+. The well-known tracer of star formation at young evolutionary stages N_2H^+ exhibits its strongest peak towards the northern region NGC 6334 I(N). However, the molecule has additional – although progressively weaker – emission peaks associated with the more evolved region NGC 6334 I. N_2H^+ emission is at a local minimum at the position of NGC 6334 E, indicating that this ion tends to avoid the H II region environment. In addition to this, N_2H^+ clearly shows extended emission, which is positionally coincident with the main filament shown in dust continuum emission (Fig. 2). Of all the spectral line species covered in this work, N_2H^+ most closely follows the dust continuum emission, showing it to be a good tracer of cold and dense material, included in star-forming regions.

HCO^+ and $H^{13}CO^+$. The HCO^+ map clearly shows its main emission peaks associated with the dense cores NGC 6334 I and I(N). It shows an additional secondary peak associated with the main carbon monoxide peaks further to the east as well as hints of the larger scale north–south ridge discussed for CO and its isotopologues above. For $H^{13}CO^+$, we cannot identify the north–south ridge anymore but the other features resemble those of the main isotopologue. It is interesting to note that the main intensity peaks for both isotopologues are associated with NGC 6334 I(N) and not the more prominent hot-core-type region NGC 6334 I. This is reminiscent to the HC_3N map published by Sollins & Megeath (2004).

CH_3OH, thermal and class I/II masers. The spectral set-up covers many CH_3OH and class I and class II maser lines as shown in Table 1 (see also Müller, Menten & Mäder 2004). It is impossible to definitively claim detection of masers given the current observations with a beam larger than 30 arcsec and a spectral resolution of a few km s^{-1}. However, we can comment on the likelihood of any transition showing masing activity, based on the relative intensities of lines at the positions of I and I(N). It is likely, then, that NGC 6334 I(N) shows maser emission in the class I transitions at 84.521 and 95.169 GHz and in the class II transition at 108.894 GHz. Val'tts et al. (2000) confirms the masing nature of the class I transition at 95.169 GHz. NGC 6334 I, on the other hand, does not show strong emission in any of the masing transitions, except perhaps the class II transition at 107.013 GHz. Cragg et al. (2001) and Val'tts et al. (1999) have both observed this class II transition towards NGC 6334 I and confirmed that it is a maser.

The thermal methanol transitions are divided into two types, based on the strength of their emission. Methanol transitions showing strong emission at 95.914, the quadruplet at 96.7 and 97.583 GHz all exhibit the bulk of their emission from NGC 6334 I(N). The methanol transitions at 100.639, 107.160 and

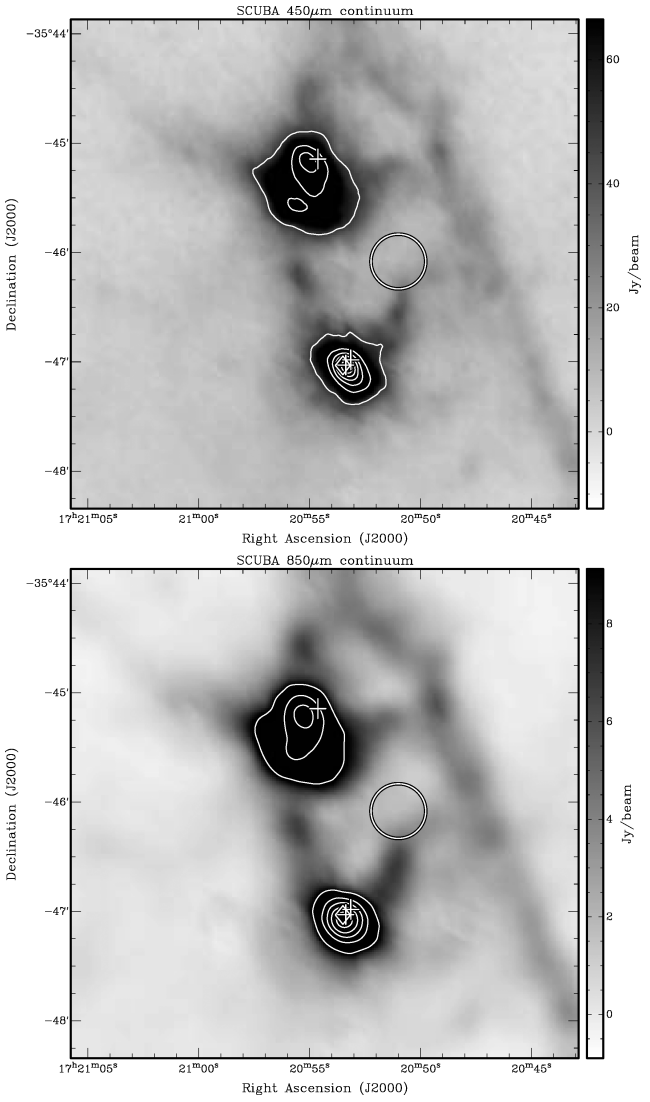

Figure 2. Dust continuum images taken with SCUBA on the JCMT, from Gören Sandell. The large circle represents the approximate size and position of the H II region NGC 6334 E (Carral et al. 2002). The diamond represents the position of the UC H II region NGC 6334 F, also known as NGC 6334 I. The two plus symbols next to the diamond represent the position of two methanol maser sites (Walsh et al. 1998). The single plus symbol in the northern half of each image represents the position of NGC 6334 I(N), traced by a methanol maser site (Walsh et al. 1998). Top: 450 μm image. The lowest contour is at 50 Jy beam^{-1} and contours are spaced at 50 Jy beam^{-1}. The peak flux density in the map is 369 Jy beam^{-1}. Bottom: 850 μm image. The lowest contour is at 10 Jy beam^{-1} and contours are spaced at 10 Jy beam^{-1}. The peak flux density in the map is 59 Jy beam^{-1}.

111.290 GHz all show weak emission that is only detected towards NGC 6334 I.

CH_3CN. Methyl cyanide is detected in the rotational transitions $J = 5_K$–4_K and 6_K–5_K. Both integrated intensity maps show two comparably strong peaks towards NGC 6334 I and I(N). Methyl cyanide is potentially useful for temperature estimates, by comparing intensity ratios of components in the K-ladders (Thorwirth et al. 2003). However, the low spectral resolutions of these data do not allow us to distinguish individual K-ladder elements. Of all the species mapped in this work, CH_3CN appears to be the one that is most concentrated towards the two regions of active star formation: NGC 6334 I and NGC 6334 I(N).

^{12}CS, ^{13}CS, $C^{34}S$ and $C^{33}S$. Carbon sulphide shows an interesting spatial variation going from the main isotopologue CS step by step through the rarer isotopologues ^{13}CS and $C^{34}S$ to $C^{33}S$. While the former main isotopologue peaks towards the southern hot-core region NGC 6334 I, the northern peak NGC 6334 I(N) is of comparable brightness for ^{13}CS and $C^{34}S$. This is likely due to the main CS isotopologue being optically thick, which is then tracing a warmer environment around NGC 6334 I. The optically thin tracers ^{13}CS and $C^{34}S$ show approximately equal brightnesses in I and I(N), suggesting that the amount of CS is approximately equal in each. However, the rare isotopologue $C^{33}S$ is brighter in I. We would expect $C^{33}S$ to look similar to ^{13}CS and $C^{34}S$. This surprising result needs to be investigated further.

SO, OCS, H_2CS and NS. Several sulphur-bearing species have been observed, and all of them show two peaks associated with NGC 6334 I and I(N). The general trend appears to be that the emission is stronger towards NGC 6334 I(N), rather than I. The one exception to this rule is OCS (8–7), where very little emission is detected towards NGC 6334 I(N), even though NGC 6334 I shows a bright peak. This is an unexpected result, especially in light of the fact that the other two OCS transitions clearly show NGC 6334 I(N) as a strong source of OCS emission.

HC_3N, HNCO, HNC, $HN^{13}C$, HCN and $H^{13}CN$. There are several hydrogen–carbon–nitrogen chain molecules observed, and all of them show two strong peaks associated with NGC 6334 I and I(N). Except for HCN where the two peaks are of approximately the same strength, in all other lines the region I(N) is clearly the dominant one. For HC_3N this has already previously been reported by Sollins & Megeath (2004). HC_3N is unusual in that it shows extended emission which appears to follow the main filament seen in dust continuum emission (Fig. 2), to the west of NGC 6334 E. Furthermore, the HC_3N emission appears to surround NGC 6334 E, but very little emission is seen inside the ring denoting the extent of this H II region. Since its morphology closely resembles that of the dust continuum emission, we find that HC_3N is a good tracer of quiescent, dense gas, as is the case for N_2H^+.

SiO. As previously reported by Megeath & Tieftrunk (1999), SiO emission is found strongly towards NGC 6334 I(N) and is weaker elsewhere in the field of view. In NGC 6334 I(N), the SiO emission is clearly associated with its molecular outflow(s) (Megeath & Tieftrunk 1999). Previous observations of the G333 giant molecular cloud (Lo et al. 2007) have found SiO emission from a region that shows similar properties to NGC 6334 I(N) with an outflow associated with a very early stage of high-mass star formation.

CH_3OCHO. The dense core tracing molecule methyl formate is detected only towards the southern hot-core region NGC 6334 I.

4.2 Comparison of NGC 6334I and I(N)

In Section 4.1, we described the morphology of emission for molecules or groups of molecules. Here we synthesize this information to present a comparison of the two star-forming sites NGC 6334 I and I(N). Based on previous work on this region (e.g. Walsh et al. 1998), it is clear that NGC 6334 I appears to be more evolved than I(N): it contains a prominent UC H II region, as well as a strong infrared source, whereas only weak radio continuum (Rodriguez, Zapata & Ho 2007) and infrared emission (Walsh et al. 1999) have been found in the vicinity of I(N). We also find evidence for an evolutionary difference in our data. Both the CS/N_2H^+ and CS/HNCO ratios are much larger for NGC 6334 I than for I(N). Previous work on the CS/N_2H^+ ratio (Zinchenko, Caselli & Pirogov 2009) and

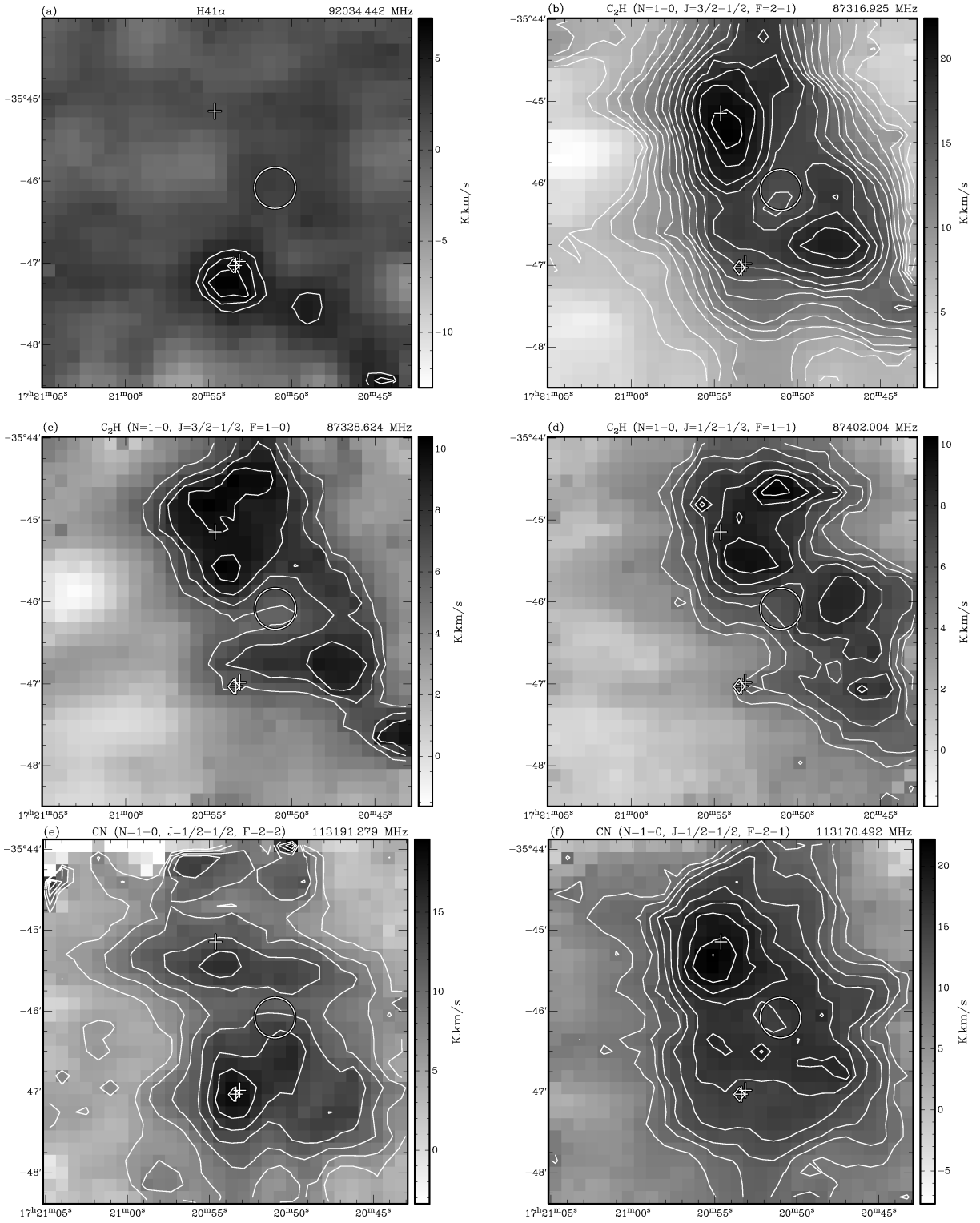

Figure 3. Integrated intensity images and contours for detected transitions. The large circle represents the approximate size and position of the H II region NGC 6334 E (Carral et al. 2002). The diamond represents the position of the UC H II region NGC 6334 F, also known as NGC 6334 I. The two plus symbols next to the diamond represent the position of two methanol maser sites (Walsh et al. 1998). The single plus symbol in the northern half of each image represents the position of NGC 6334 I(N), traced by a methanol maser site (Walsh et al. 1998). Axes are labelled in coordinates of RA and Dec. (J2000). The intensity scale is in units of brightness temperature multiplied by velocity. (a) H41α radio recombination line. Contours start at 5σ and increase in 1σ steps, where 1σ is 0.9 K km s^{-1}. (b) C_2H ($N = 1$–0, $J = 3/2$–$1/2$, $F = 2$–1) – ethynyl radical. Contours start at 5σ and increase in 1σ steps, where 1σ is 1.2 K km s^{-1}. (c) C_2H ($N = 1$–0, $J = 3/2$–$1/2$, $F = 1$–0) – ethynyl radical. Contours start at 5σ and increase in 1σ steps, where 1σ is 1.2 K km s^{-1}. (d) C_2H ($N = 1$–0, $J = 1/2$–$1/2$, $F = 1$–1) – ethynyl radical. Contours start at 5σ and increase in 1σ steps, where 1σ is 0.9 K km s^{-1}. (e) CN ($N = 1$–0, $J = 1/2$–$1/2$, $F = 2$–2) – cyanogen radical. Contours start at 5σ and increase in 2σ steps, where 1σ is 1.1 K km s^{-1}. Note that this transition was particularly sensitive to weather. Features in the northern quarter of the image [north of I(N)] are almost certainly a result of poor weather and not real. (f) CN ($N = 1$–0, $J = 1/2$–$1/2$, $F = 2$–1) – cyanogen radical. Contours start at 5σ and increase in 1σ steps, where 1σ is 1.7 K km s^{-1}.

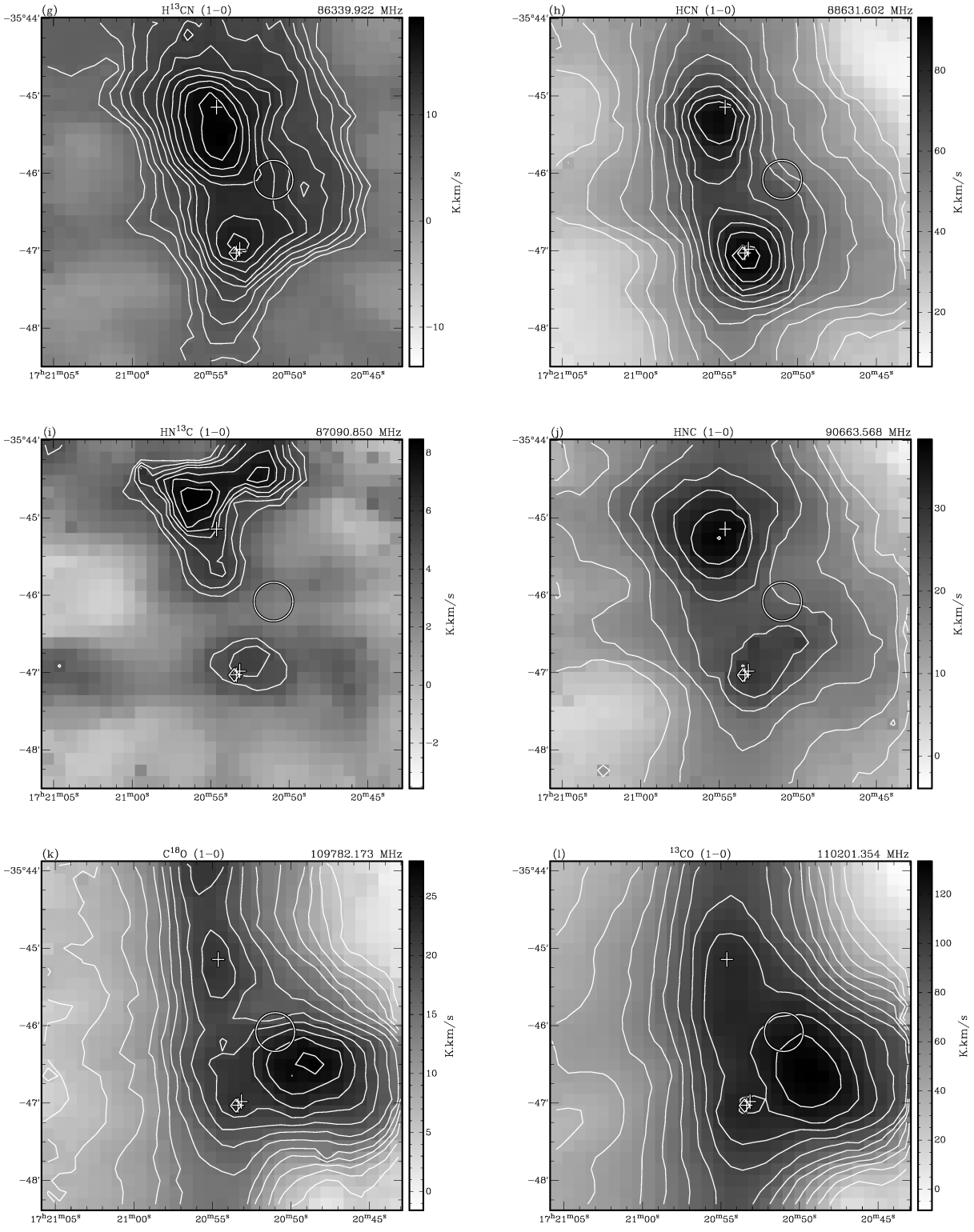

Figure 3 – *continued* (g) $H^{13}CN$ (1–0) – hydrogen cyanide. Contours start at 5σ and increase in 1σ steps, where 1σ is $1.2\,\mathrm{K\,km\,s^{-1}}$. (h) HCN (1–0) – hydrogen cyanide. Contours start at 5σ and increase in 1σ steps, where 1σ is $6.0\,\mathrm{K\,km\,s^{-1}}$. (i) $HN^{13}C$ (1–0) – hydrogen isocyanide. Contours start at 5σ and increase in 1σ steps, where 1σ is $0.6\,\mathrm{K\,km\,s^{-1}}$. (j) HNC (1–0) – hydrogen isocyanide. Contours start at 5σ and increase in 2σ steps, where 1σ is $2.0\,\mathrm{K\,km\,s^{-1}}$. (k) $C^{18}O$ (1–0) – carbon monoxide. Contours start at 5σ and increase in 2σ steps, where 1σ is $1.1\,\mathrm{K\,km\,s^{-1}}$. (l) ^{13}CO (1–0) – carbon monoxide. Contours start at 5σ and increase in 2σ steps, where 1σ is $5.0\,\mathrm{K\,km\,s^{-1}}$.

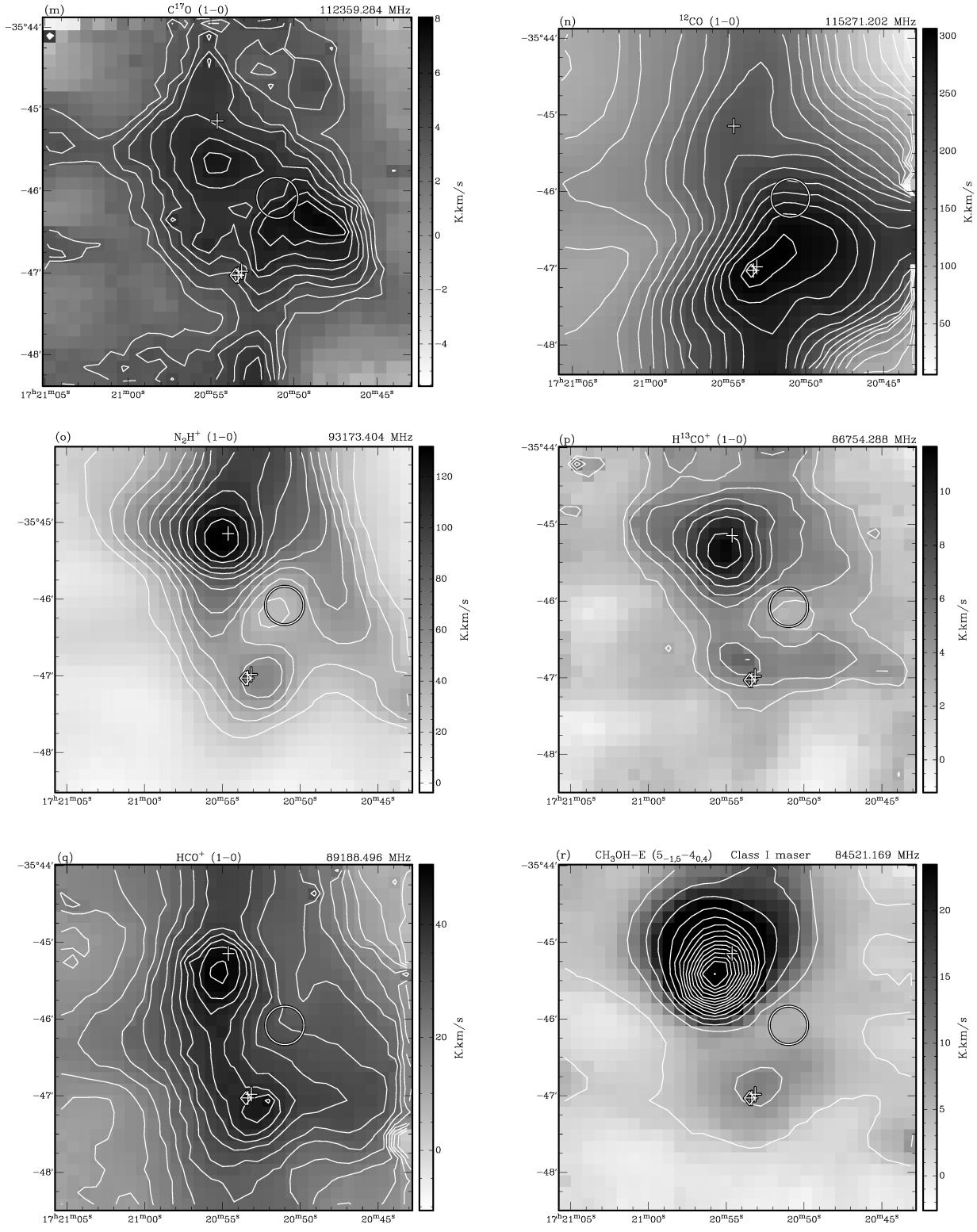

Figure 3 – *continued* (m) $C^{17}O$ (1–0) – carbon monoxide. Contours start at 5σ and increase in 1σ steps, where 1σ is 0.6 K km s^{-1}. (n) ^{12}CO (1–0) – carbon monoxide. Contours start at 5σ and increase in 3σ steps, where 1σ is 5.0 K km s^{-1}. (o) N_2H^+ (1–0) – diazenylium. Contours start at 5σ and increase in 2σ steps, where 1σ is 5.0 K km s^{-1}. (p) $H^{13}CO^+$ (1–0) – oxomethylium. Contours start at 5σ and increase in 2σ steps, where 1σ is 0.6 K km s^{-1}. (q) HCO^+ (1–0) – oxomethylium. Contours start at 5σ and increase in 2σ steps, where 1σ is 1.6 K km s^{-1}. (r) CH_3OH-E ($5_{-1,5}$–$4_{0,4}$) – methanol. Contours start at 5σ and increase in 10σ steps, where 1σ is 0.6 K km s^{-1}. This methanol transition is a class I maser (Müller et al. 2004).

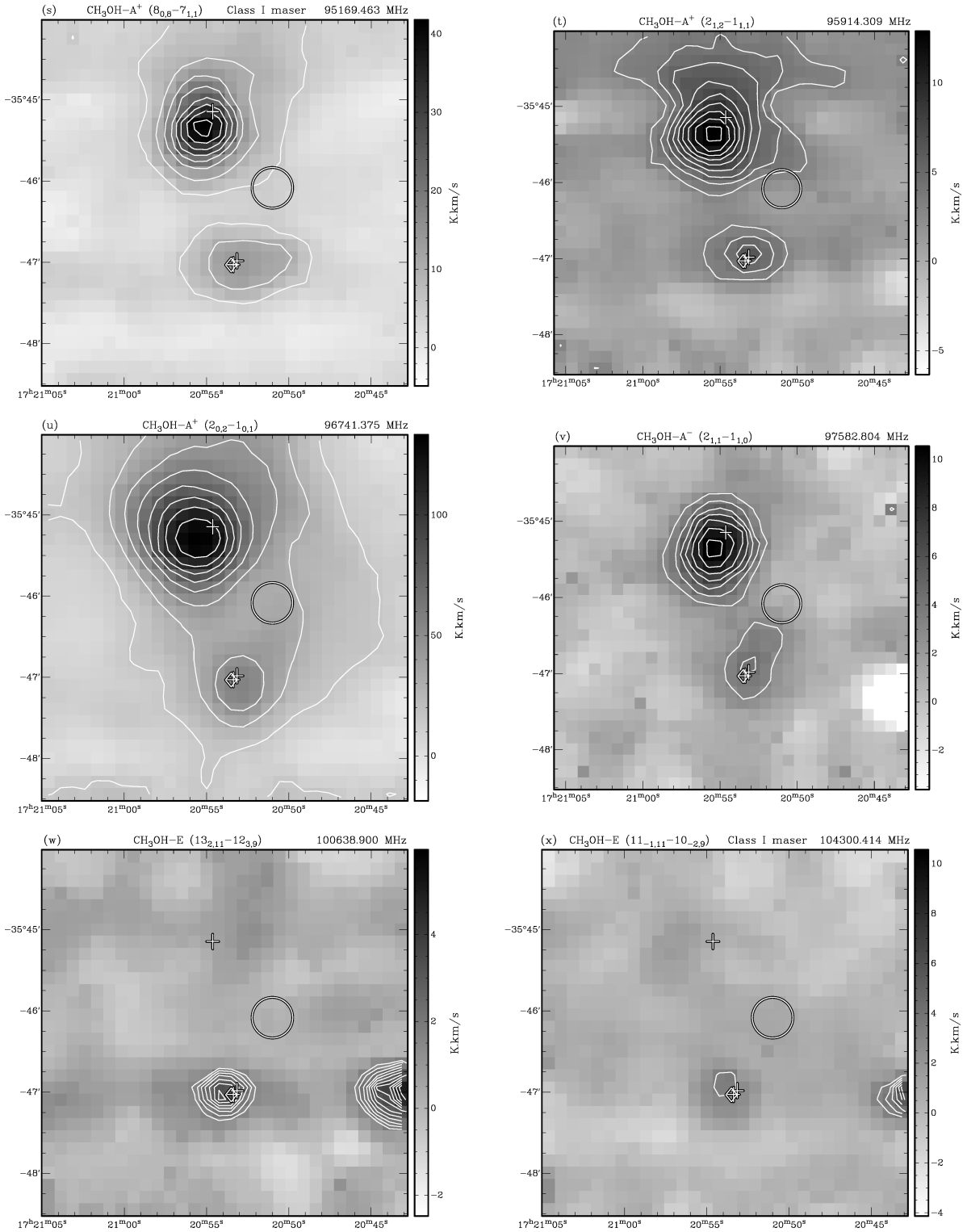

Figure 3 – *continued* (s) CH_3OH-A^+ ($8_{0,8}$–$7_{1,7}$) – methanol. Contours start at 5σ and increase in 5σ steps, where 1σ is $1.0\,K\,km\,s^{-1}$. This methanol transition is a class I maser (Müller et al. 2004). (t) CH_3OH-A^+ ($2_{1,2}$–$1_{1,1}$) – methanol. Contours start at 5σ and increase in 2σ steps, where 1σ is $0.6\,K\,km\,s^{-1}$. (u) CH_3OH-A^+ ($2_{0,2}$–$1_{0,1}$) – methanol. Contours start at 5σ and increase in 5σ steps, where 1σ is $3.0\,K\,km\,s^{-1}$. (v) CH_3OH-A^- ($2_{1,1}$–$1_{1,0}$) – methanol. Contours start at 5σ and increase in 2σ steps, where 1σ is $0.6\,K\,km\,s^{-1}$. (w) CH_3OH-E ($13_{2,11}$–$12_{3,9}$) – methanol. Contours start at 5σ and increase in 1σ steps, where 1σ is $0.3\,K\,km\,s^{-1}$. Strong 'emission' is seen on the right-hand edge of the image, at a declination of approximately $-35°47'$, which is due to a bad data point, and is not real emission. (x) CH_3OH-E ($11_{-1,11}$–$10_{-2,9}$) – methanol. Contours start at 5σ and increase in 1σ steps, where 1σ is $0.6\,K\,km\,s^{-1}$. This methanol transition is a class I maser (Müller et al. 2004). 'Emission' is seen on the right-hand edge of the image, at a declination of approximately $-35°47'$, which is due to a bad data point, and is not real emission.

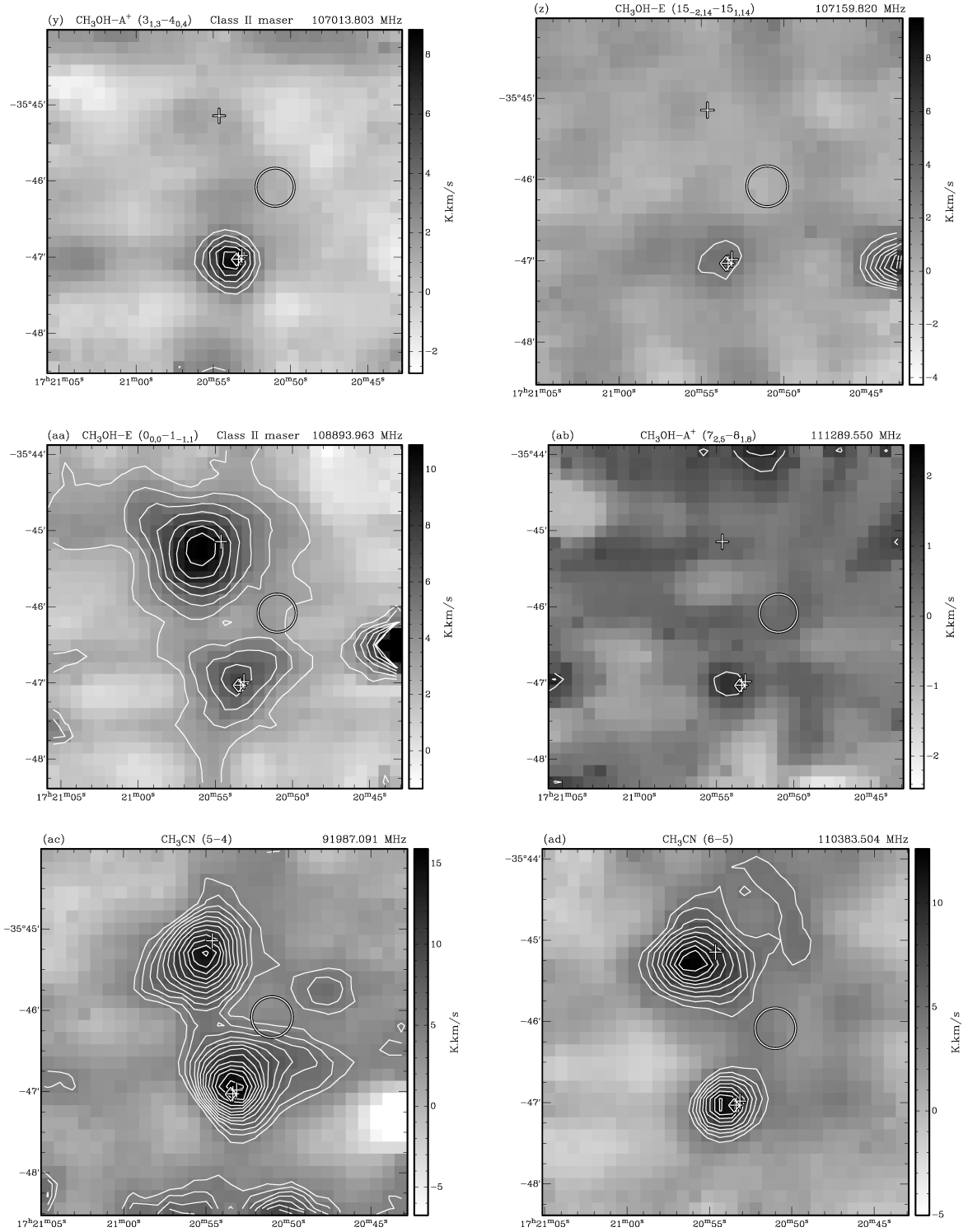

Figure 3 – *continued* (y) CH_3OH-A^+ ($3_{1,3}$–$4_{0,4}$) – methanol. Contours start at 5σ and increase in 2σ steps, where 1σ is $0.6\,K\,km\,s^{-1}$. This methanol transition is a class II maser (Müller et al. 2004). (z) CH_3OH-E ($15_{-2,14}$–$15_{1,14}$) – methanol. Contours start at 5σ and increase in 1σ steps, where 1σ is $0.6\,K\,km\,s^{-1}$. Strong 'emission' is seen on the right-hand edge of the image, at a declination of approximately $-35°47'$, which is due to a bad data point, and is not real emission. (aa) CH_3OH-E ($0_{0,0}$–$1_{-1,1}$) – methanol. Contours start at 5σ and increase in 2σ steps, where 1σ is $0.6\,K\,km\,s^{-1}$. This methanol transition is a class II maser (Müller et al. 2004). Strong "mission' is seen on the right-hand edge of the image, at a declination of approximately $-35°46'30''$, which is due to a bad data point, and is not real emission. (ab) CH_3OH-A^+ ($7_{2,5}$–$8_{1,8}$) – methanol. Contours start at 3σ and increase in 1σ steps, where 1σ is $0.5\,K\,km\,s^{-1}$. (ac) CH_3CN (5–4) – methyl cyanide. The emission includes all transitions in the *K*-ladder from 0 to 3, inclusive. Contours start at 5σ and increase in 1σ steps, where 1σ is $0.9\,K\,km\,s^{-1}$. We attribute the 'emission' seen south of $-35°48'$ to be due to poor weather and is thus not real. (ad) CH_3CN (6–5) – methyl cyanide. The emission includes all transitions in the *K*-ladder from 0 to 3, inclusive. Contours start at 5σ and increase in 1σ steps, where 1σ is $0.9\,K\,km\,s^{-1}$.

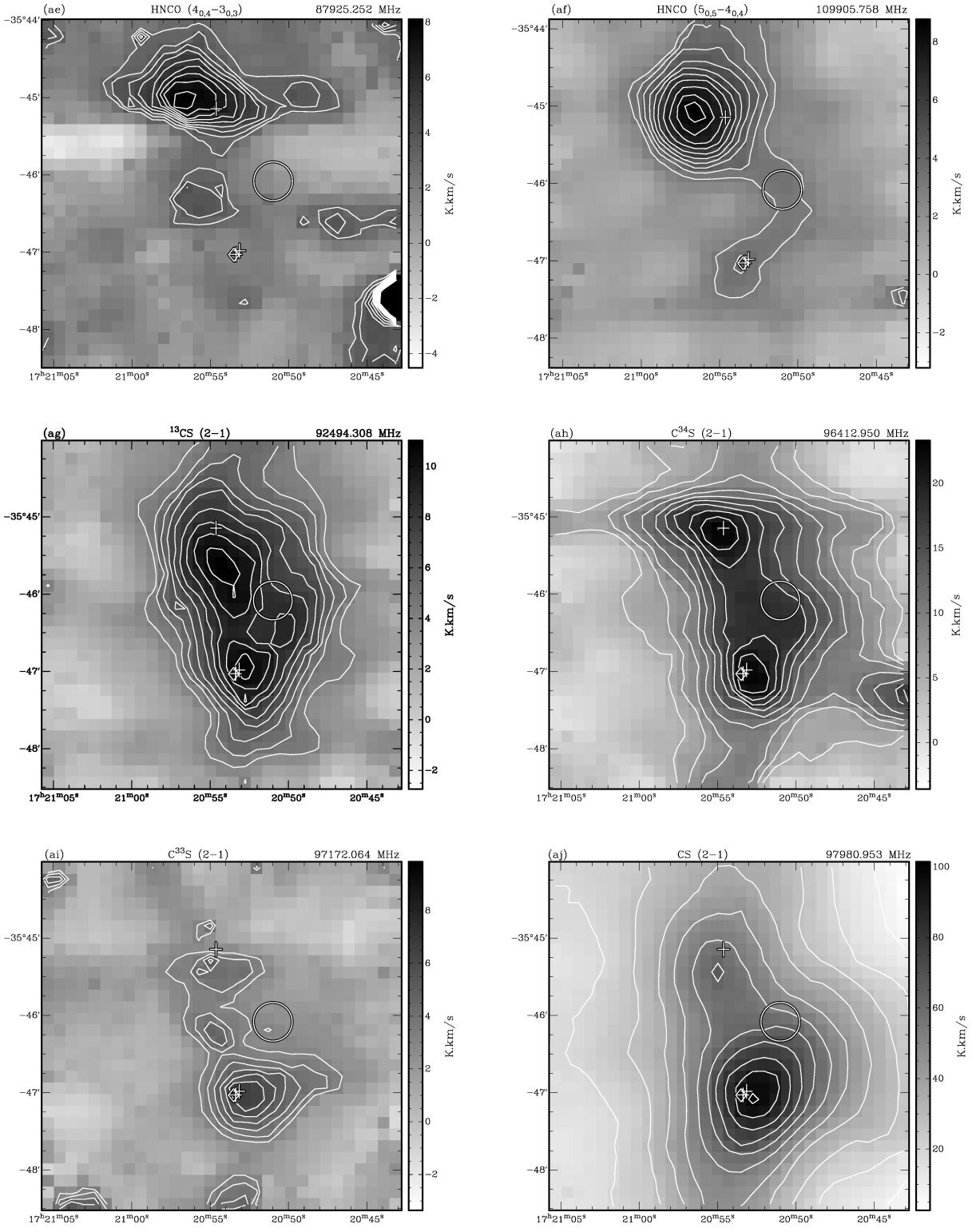

Figure 3 – *continued* (ae) HNCO ($4_{0,4}$–$3_{0,3}$) – isocyanic acid. Contours start at 5σ and increase in 1σ steps, where 1σ is 0.6 K km s^{-1}. Strong 'emission' is seen on the right-hand edge of the image, at a declination of approximately −35°47′30″, which is due to a bad data point, and is not real emission. (af) HNCO ($5_{0,5}$–$4_{0,4}$) – isocyanic acid. Contours start at 5σ and increase in 1σ steps, where 1σ is 0.6 K km s^{-1}. (ag) ^{13}CS (2–1) – carbon sulphide. Contours start at 5σ and increase in 1σ steps, where 1σ is 0.7 K km s^{-1}. (ah) C^{34}S (2–1) – carbon sulphide. Contours start at 5σ and increase in 2σ steps, where 1σ is 1.0 K km s^{-1}. Strong 'emission' is seen on the right-hand edge of the image, at a declination of approximately −35°47′15″, which is due to a bad data point, and is not real emission. (ai) C^{33}S (2–1) – carbon sulphide. Contours start at 5σ and increase in 1σ steps, where 1σ is 0.6 K km s^{-1}. (aj) CS (2–1) – carbon sulphide. Contours start at 5σ and increase in 5σ steps, where 1σ is 1.8 K km s^{-1}.

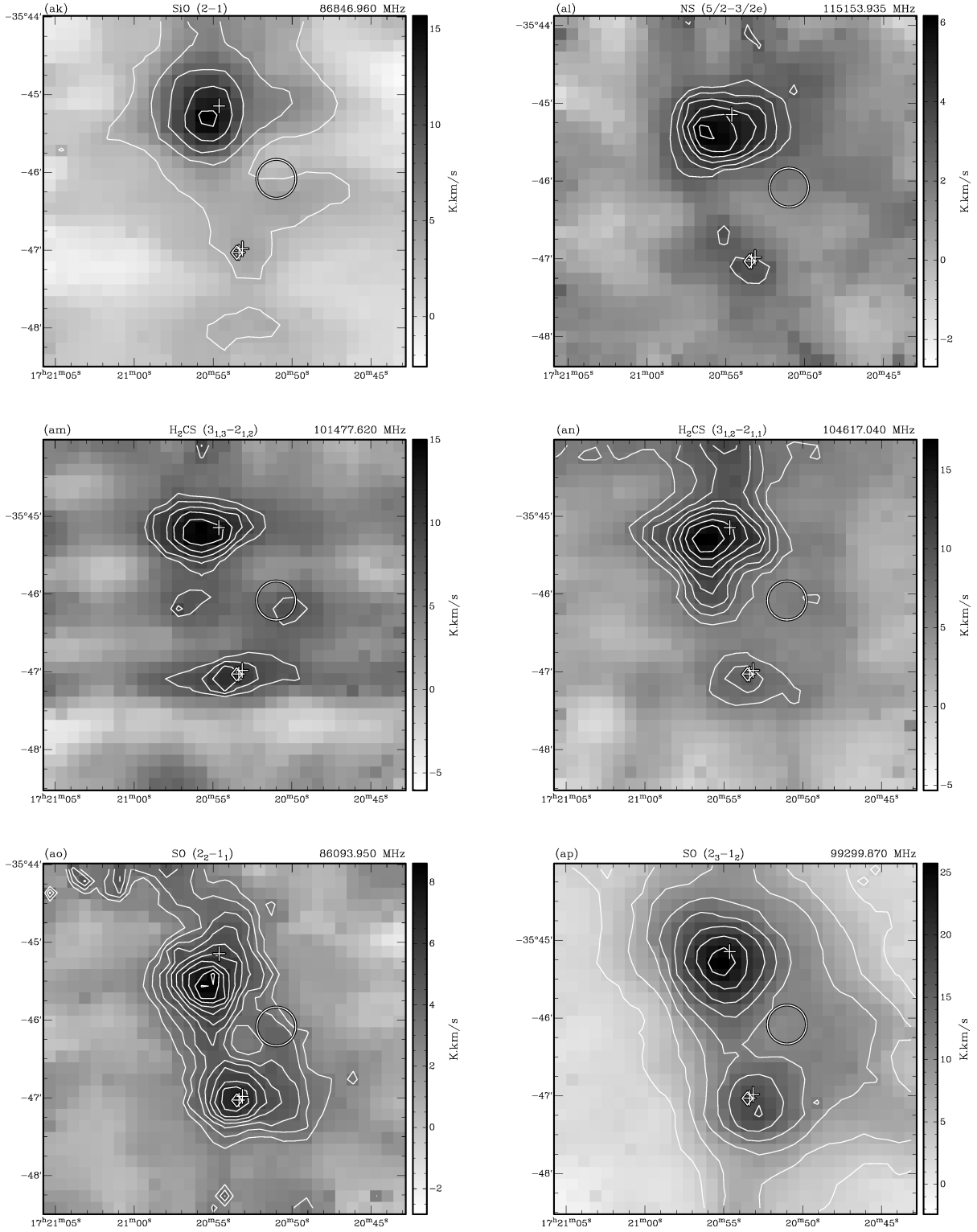

Figure 3 – *continued* (ak) SiO (2–1) – silicon monoxide. Contours start at 5σ and increase in 5σ steps, where 1σ is $0.6\,\mathrm{K\,km\,s^{-1}}$. (al) NS (5/2–3/2e) – nitrogen sulphide. Contours start at 5σ and increase in 1σ steps, where 1σ is $0.6\,\mathrm{K\,km\,s^{-1}}$. (am) H_2CS ($3_{1,3}$–$2_{1,2}$) – thioformaldehyde. Contours start at 5σ and increase in 1σ steps, where 1σ is $1.5\,\mathrm{K\,km\,s^{-1}}$. (an) H_2CS ($3_{1,2}$–$2_{1,1}$) – thioformaldehyde. Contours start at 5σ and increase in 1σ steps, where 1σ is $1.3\,\mathrm{K\,km\,s^{-1}}$. (ao) SO ($2_2$–$1_1$) – sulphur monoxide. Contours start at 5σ and increase in 1σ steps, where 1σ is $0.6\,\mathrm{K\,km\,s^{-1}}$. (ap) SO ($2_3$–$1_2$) – sulphur monoxide. Contours start at 5σ and increase in 5σ steps, where 1σ is $0.6\,\mathrm{K\,km\,s^{-1}}$.

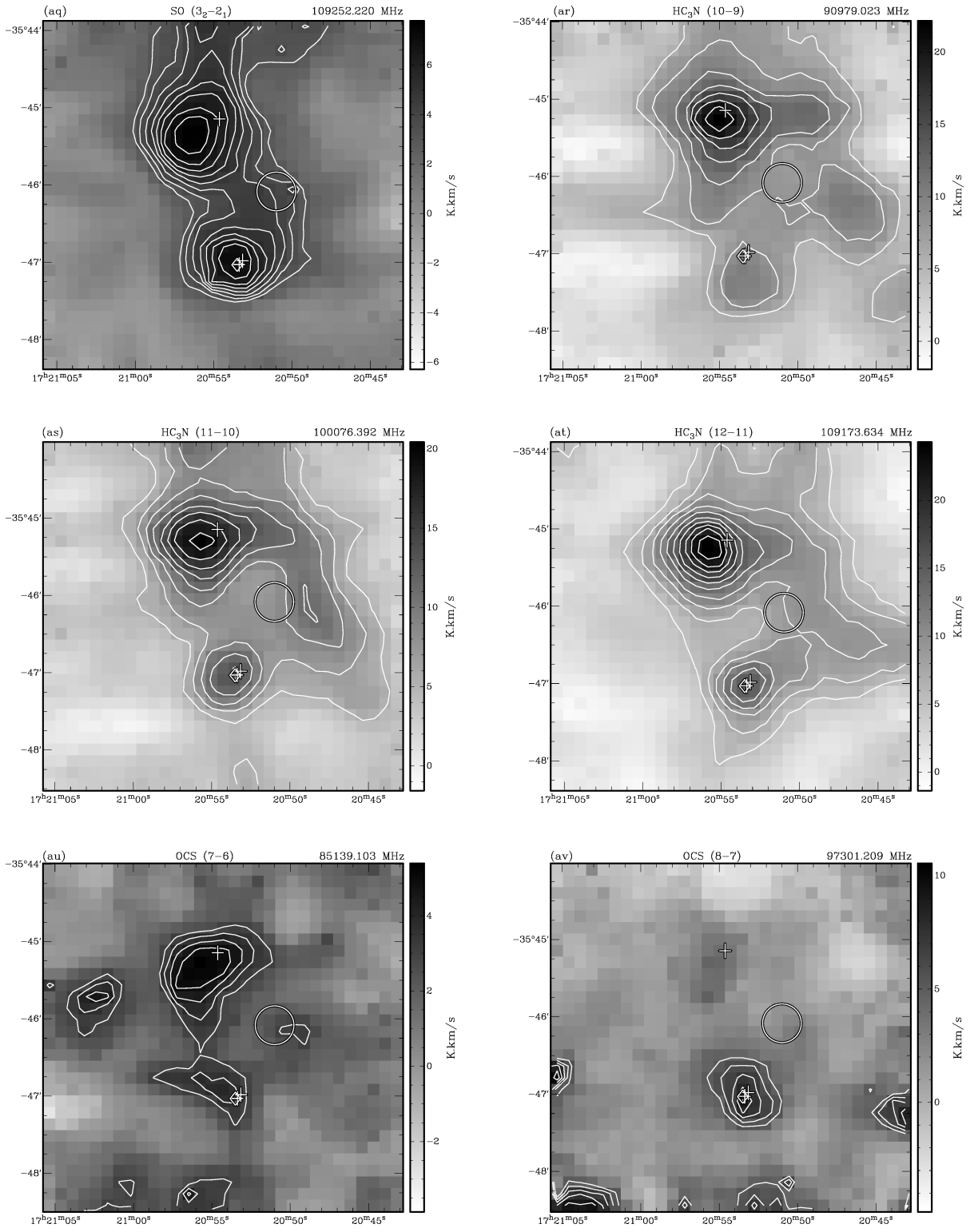

Figure 3 – *continued* (aq) SO (3_2–2_1) – sulphur monoxide. Contours start at 5σ and increase in 1σ steps, where 1σ is 0.6 K km s^{-1}. (ar) HC_3N (10–9) – cyanoacetylene. Contours start at 5σ and increase in 2σ steps, where 1σ is 1.2 K km s^{-1}. (as) HC_3N (11–10) – cyanoacetylene. Contours start at 5σ and increase in 2σ steps, where 1σ is 1.1 K km s^{-1}. (at) HC_3N (12–11) – cyanoacetylene. Contours start at 5σ and increase in 2σ steps, where 1σ is 1.1 K km s^{-1}. (au) OCS (7–6) – carbonyl sulphide. Contours start at 5σ and increase in 1σ steps, where 1σ is 0.6 K km s^{-1}. (av) OCS (8–7) – carbonyl sulphide. Contours start at 5σ and increase in 1σ steps, where 1σ is 1.1 K km s^{-1}. Strong 'emission' is seen around edges of the bottom half of the image, which is most likely due to poor weather, and is not real emission.

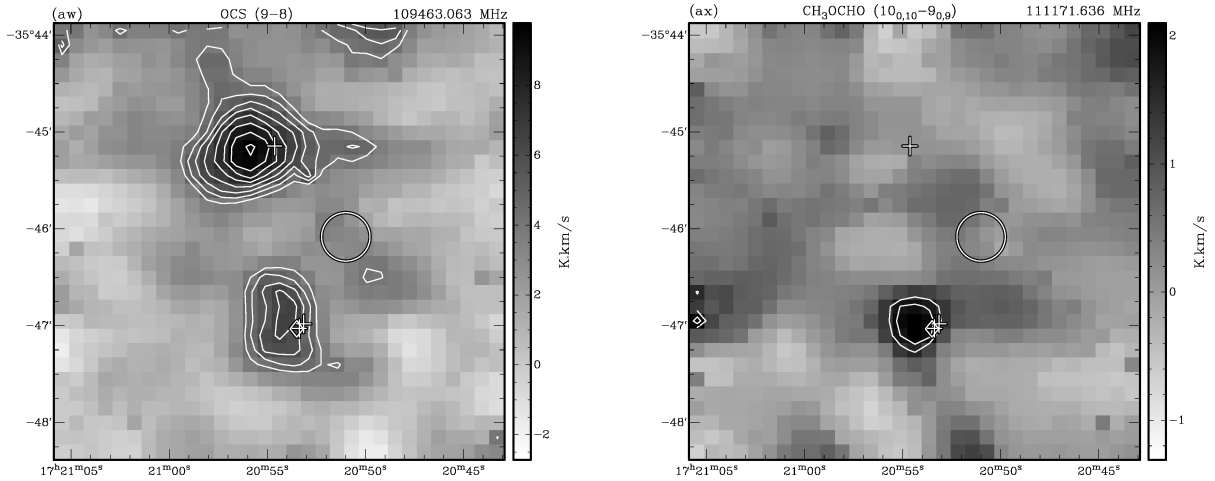

Figure 3 – *continued* (aw) OCS (9–8) – carbonyl sulphide. Contours start at 5σ and increase in 1σ steps, where 1σ is $0.7\,\mathrm{K\,km\,s^{-1}}$. 'Emission' is seen around the northern edge of the image, which is most likely due to poor weather, and is not real emission. (ax) CH_3OCHO-A ($10_{0,10}$–$9_{0,9}$) – methyl formate. Contours start at 5σ and increase in 1σ steps, where 1σ is $0.3\,\mathrm{K\,km\,s^{-1}}$.

CS/HNCO ratio (Martín et al. 2008) have indicated that CS is likely to be enhanced in abundance towards photodissociation regions (PDRs), whilst both N_2H^+ and HNCO are likely to be reduced in abundance towards PDRs. Thus, NGC 6334 I shows PDR-like ratios, presumably due to the UC H II region, whereas abundances of both N_2H^+ and HNCO do not appear to be reduced, compared to CS in NGC 6334 I(N), where a PDR is yet to form.

When comparing the non-masing lines of CH_3OH, we find that the emission is stronger towards NGC 6334 I in the 100.638, 107.159 and 111.289 GHz transitions. CH_3OH emission is stronger towards NGC 6334 I(N) in the 95.915, 96.741 (quadruplet) and 97.582 GHz transitions. The stronger transitions in NGC 6334 I all have upper energy levels between 103 and 304 K, whilst all the stronger transitions in NGC 6334 I(N) have upper energy levels no greater than 22 K. Thus, we can attribute the stronger emission in NGC 6334 I to hot CH_3OH and the stronger emission in NGC 6334 I(N) to cold CH_3OH emission. Whilst previous work has shown that both NGC 6334 I and I(N) have hot components, with temperatures in excess of 400 K (Beuther et al. 2007), it is clear that the large-scale CH_3OH observed here has only had time to heat up in NGC 6334 I.

We detect CH_3OCHO only towards NGC 6334 I. This molecule is thought to be produced only after a young star or protostar has heated up the surrounding material to above 100 K (Garrod & Herbst 2006). This provides further evidence of the more evolved state of NGC 6334 I over that of I(N).

4.3 Line ratio maps

The ratio of integrated intensities for different spectral lines can potentially be used to identify physical and chemical characteristics of regions within the map. For example, a simple comparison of ratios for different lines of the same species might be used to map physical quantities such as density and temperature. However, most species detected in multiple spectral lines (i.e. CN, CH_3CN, HNCO, SO, HC_3N and OCS) show only a narrow range of energy levels over the multiple spectral lines. Thus, only small changes in line ratios are expected from different spectral lines of the same species. In addition to this, small differences in the relative position of maps made at different frequencies can lead to artefacts that can dominate line ratios. In the present study, these complicating factors make such line ratio maps too unreliable to interpret. The only exception to this is CH_3OH, where clear differences in the intensities of lines are seen between NGC 6334 I and I(N), as discussed in Section 4.1.

It is possible to compare line ratios between species that have been observed simultaneously, as this eliminates any relative positional offsets as well as any varying effects of weather. In Fig. 4, we show images based on the ratio of line-integrated intensities for different species.

The upper left image shows the $C^{18}O/^{12}CO$ line ratio map. The highest ratio is found surrounding NGC 6334 I(N). A high ratio between these two lines means that the ^{12}CO line is optically thick. We also see a secondary peak in the ratio to the south-west of NGC 6334 E, which is close to the ^{12}CO peak-integrated intensity (shown in contours). At this position, it is likely that there is a high column density of gas. At NGC 6334 I, the line ratio is relatively low. The ^{12}CO gas is likely optically thick here since it is one of the centres of high column density gas in many other lines. The relatively low ratio, compared to that found in NGC 6334 I(N), indicates that the ^{12}CO emission is likely to be optically thick along most lines of sight covered in these observations.

The upper right image shows the $HNCO/C^{18}O$ line ratio map. As mentioned in Section 4.2, HNCO tends to be destroyed in PDRs. Thus, the line ratio map broadly shows two regions in the map: a region to the east of NGC 6334 I(N), which shows a high ratio (i.e. not a PDR), and a region including NGC 6334 I and E, which appears to be a good candidate PDR, although a low signal in HNCO limits our interpretation beyond a narrow strip joining NGC 6334 I and E.

The lower left image shows the CH_3CN/N_2H^+ line ratio map. As mentioned in Section 4.1, the CH_3CN emission is strongly confined to the centres of active star formation: NGC 6334 I and I(N), whereas N_2H^+ tends to trace ubiquitous and quiescent gas. The line ratio map clearly shows a low line ratio towards NGC 6334 I, in contrast to a high ratio seen at NGC 6334 I(N). This demonstrates that I(N) is a more quiescent region, presumably with star formation at a younger stage.

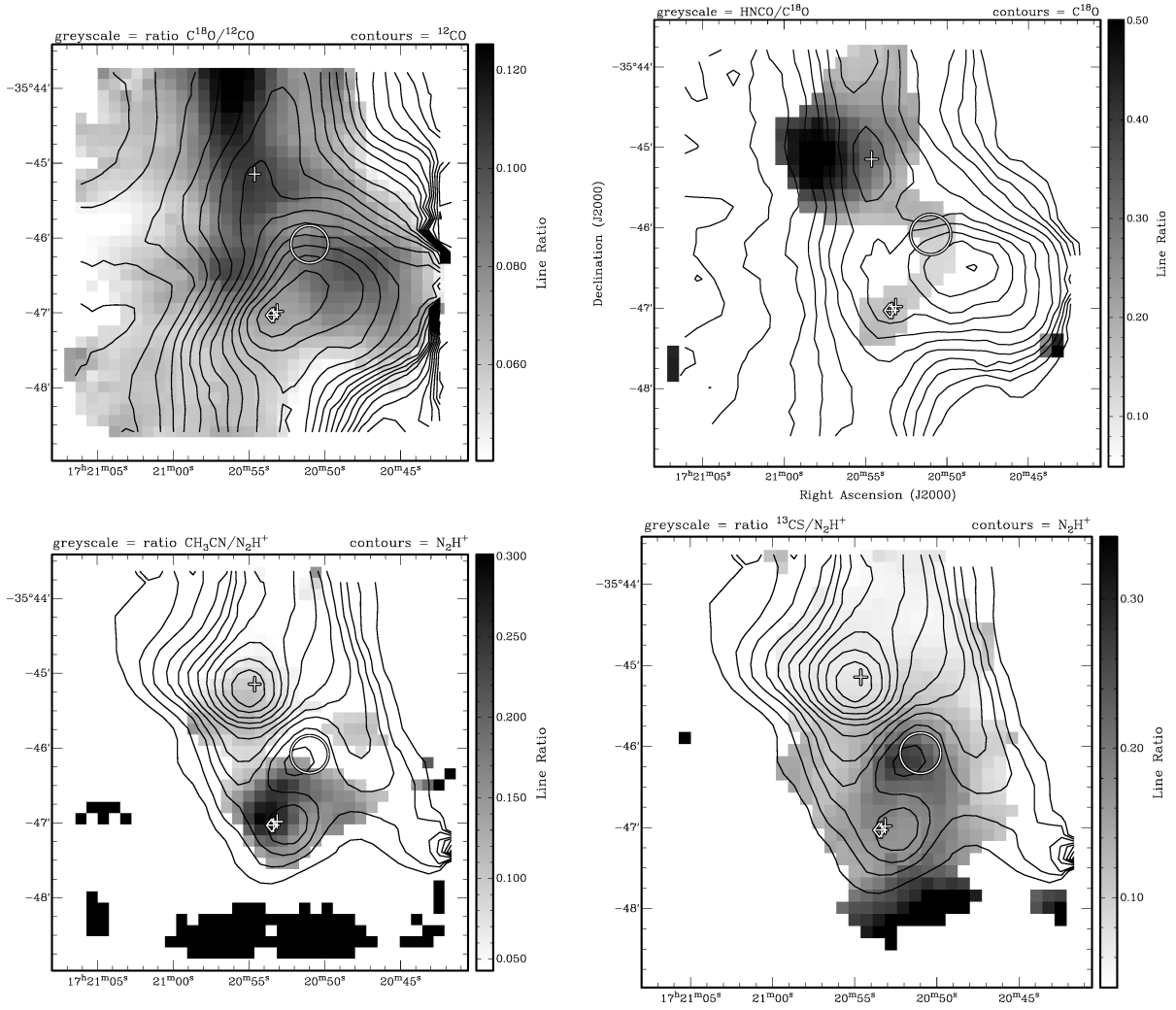

Figure 4. Line ratio maps. Upper left: the $C^{18}O$ (1–0)/^{12}CO (1–0) ratio in grey-scale and ^{12}CO (1–0) integrated intensity in contours. Upper right: the HNCO ($5_{0,5}$–$4_{0,4}$)/$C^{18}O$ (1–0) ratio in grey-scale and $C^{18}O$ (1–0) integrated intensity in contours. Lower left: the CH_3CN (5–4)/N_2H^+ (1–0) ratio in grey-scale and N_2H^+ integrated intensity in contours. Lower right: the ^{13}CS (2–1)/N_2H^+ (1–0) ratio in grey-scale and N_2H^+ (1–0) integrated intensity in contours. Dark areas show high line ratios and light areas show low line ratios. The same contour levels as for Fig. 3 have been used. Each ratio map is masked, based on the weaker image (the numerator), to reduce contributions due to non-real emission. However, non-real emission is seen at the bottom of the line ratio map for the CH_3CN/N_2H^+ map below the N_2H^+ contours.

The lower right image shows the ^{13}CS/N_2H^+ line ratio map. Here, we see the highest line ratio at the position of the H II region NGC 6334 E. This is probably the result of N_2H^+ being destroyed by the H II region.

5 CONCLUSIONS

We have mapped a 5 × 5 arcmin^2 region, encompassing the high-mass star formation sites NGC 6334 I and I(N). We have covered most of the 3 mm spectral window with these observations, using the Mopra radio telescope. Our observations do not have sufficient spectral resolution to resolve spectral lines, but we compare morphologies of the various lines detected. We detect emission from 19 different molecules, ions and radicals, including multiple transitions of the same species and transitions from various isotopologues to yield a total of 52 spectral line detections.

We find that CH_3CN most closely follows the sites of active star formation, although these sites feature prominently most other observed species. In contrast, emission from both CN and C_2H appears to be widespread and are good tracers of gas that is not associated with active star formation. N_2H^+ and HC_3N morphologies closely resemble that of dust continuum emission, indicating that these two species are good tracers of column density, associated with both star-forming sites and quiescent gas.

It is difficult to interpret the emission from common species and their isotopologues (i.e. CO, HCO^+, HCN and HNC), which is likely due to some transitions being optically thick. All CO isotopologues show a peak of emission about 45 arcsec to the south-west of the H II region NGC 6334 E. However, this peak is not prominent in any other tracer, including dust continuum emission. We are currently unable to provide an explanation for this.

CH_3OH emission is seen in many transitions, including known class I and II masers. Due to the low spatial resolution of these observations, we cannot conclude that we have detected any new masers amongst these new transitions. Thermal CH_3OH transitions show a marked difference in their occurrence: transitions with upper level kinetic temperatures above 100 K are found to be stronger towards

NGC 6334 I and transitions with upper level kinetic temperatures below 22 K are found to be stronger towards NGC 6334 I(N). This supports the interpretation that NGC 6334 I is a more evolved site for star formation than I(N).

ACKNOWLEDGMENTS

The authors would like to thank Göran Sandell for providing the SCUBA continuum images shown in Fig. 2. The Mopra telescope is part of the Australia Telescope and is funded by the Commonwealth of Australia for operation as a National Facility managed by CSIRO. The University of New South Wales Mopra Spectrometer Digital Filter Bank used for the observations with the Mopra telescope was provided with support from the Australian Research Council, together with the University of New South Wales, University of Sydney, Monash University and the CSIRO. HB acknowledges financial support by the Emmy Noether Programme of the Deutsche Forschungsgemeinschaft (DFG, grant BE2578). The authors would like to thank the anonymous referee whose comments and suggestions have greatly improved the quality of this paper.

REFERENCES

Bachiller R., Cernicharo J., 1990, ApJ, 239, 276
Beuther H., Thorwirth S., Zhang Q., Hunter T. R., Megeath S. T., Walsh A. J., Menten K. M., 2005, ApJ, 627, 834
Beuther H., Walsh A. J., Thorwirth S., Zhang Q., Hunter T. R., Megeath S. T., Menten K. M., 2007, A&A, 466, 989
Beuther H., Semenov D., Henning Th., Linz H., 2008, ApJ, 675, L33
Carral P., Kurtz S. E., Rodríguez L. F., Menten K., Cantó J., Arceo R., 2002, AJ, 123, 2574
Cheung L., Frogel J. A., Hauser M. G., Gezari D. Y., 1978, ApJ, 226, L149
Cragg D. M., Sobolev A. M., Ellingsen S. P., Caswell J. L., Godfrey P. D., Salii S. V., Dodson R. G., 2001, MNRAS, 323, 939
Garrod R. T., Herbst E., 2006, A&A, 457, 927
Gezari D. Y., 1982, ApJ, 259, L29
Herbst E., Leung C. M., 1986, MNRAS, 222, 689
Hunter T. R., Brogan C. L., Megeath S. T., Menten K. M., Beuther H., Thorwirth S., 2006, ApJ, 649, 888
Kraemer K. E., Jackson J. M., 1999, ApJS, 124, 439
Ladd N., Purcell C., Wong T., Robertson S., 2005, Publ. Astron. Soc. Australia, 22, 62
Leurini S., Schilke P., Parise B., Wyrowski F., Güsten R., Philipp S., 2006, A&A, 454, L83
Lo N., Cunningham M., Bains I., Burton M. G., Garay G., 2007, MNRAS, 381, L30
McBreen B., Fazio G. G., Stier M., Wright E. L., 1979, ApJ, 232, L183
McCutcheon W. H., Sandell G., Matthews H. E., Kuiper T. B. H., Sutton E. C., Danchi W. C., Sato T., 2000, MNRAS, 316, 152
Martín S., Requena-Torres M. A., Martín-Pintado J., Mauersberger R., 2008, ApJ, 678, 245
Megeath S. T., Tieftrunk A. R., 1999, ApJ, 526, L113
Millar T. J., Nejad L. A. M., 1985, MNRAS, 217, 507
Müller H. S. P., Thorwirth S., Roth D. A., Winnewisser G., 2001, A&A, 370, L49
Müller H. S. P., Menten K. M., Mäder H., 2004, A&A, 428, 1019
Müller H. S. P., Schlöder F., Stutzki J., Winnewisser G., 2005, J. Molecular Structure, 742, 215
Neckel T., 1978, A&A, 69, 51
Pickett H. M., Poynter R. L., Cohen E. A., Delitsky M. L., Pearson J. C., Müller H. S. P., 1998, J. Quant. Spectrosc. Radiative Transfer, 60, 883
Rodriguez L. F., Canto J., Moran J. M., 1982, ApJ, 255, 103
Rodriguez L. F., Zapata L. A., Ho P. T. P., 2007, ApJ, 654, L143
Sandell G., 2000, A&A, 358, 242
Schilke P., Comito C., Thorwirth S., Wyrowski F., Menten K. M., Güsten R., Bergman P., Nyman L.-Å., 2006, A&A, 454, L41
Sollins P. K., Megeath S. T., 2004, AJ, 128, 2374
Thorwirth S., Winnewisser G., Megeath S. T., Tieftrunk A. R., 2003, in De Buizer J. M., van der Bliek N. S., eds, ASP Conf. Ser. Vol. 287, Galactic Star Formation Across the Stellar Mass Spectrum. Astron. Soc. Pac., San Francisco, p. 257
Turner B. E., Terzieva R., Herbst E., 1999, ApJ, 518, 699
Val'tts I. E., Ellingsen S. P., Slysh V. I., Kalenskii S. V., Otrupcek R., Voronkov M. A., 1999, MNRAS, 310, 1077
Val'tts I. E., Ellingsen S. P., Slysh V. I., Kalenskii S. V., Otrupcek R., Larionov G. M., 2000, MNRAS, 317, 315
Walsh A. J., Burton M. G., Hyland A. R., Robinson G., 1998, MNRAS, 301, 640
Walsh A. J., Burton M. G., Hyland A. R., Robinson G., 1999, MNRAS, 309, 905
Zinchenko I., Caselli P., Pirogov L., 2009, MNRAS, 395, 2234

This paper has been typeset from a TEX/LATEX file prepared by the author.